Journal of Maps

ISSN: (Print) (Online) Journal homepage: https://www.tandfonline.com/loi/tjom20

Morphology of the submerged Ferdinandea Island, the 'Neverland' of the Sicily Channel (central Mediterranean Sea)

Daniele Spatola, Attilio Sulli, Luca Basilone, Daniele Casalbore, Simone Napoli, Gualtiero Basilone & Francesco Latino Chiocci

To cite this article: Daniele Spatola, Attilio Sulli, Luca Basilone, Daniele Casalbore, Simone Napoli, Gualtiero Basilone & Francesco Latino Chiocci (2023) Morphology of the submerged Ferdinandea Island, the 'Neverland' of the Sicily Channel (central Mediterranean Sea), Journal of Maps, 19:1, 2243305, DOI: 10.1080/17445647.2023.2243305

To link to this article: https://doi.org/10.1080/17445647.2023.2243305

JOURNAL OF MAPS
2023, VOL. 19, NO. 1, 2243305
https://doi.org/10.1080/17445647.2023.2243305

Morphology of the submerged Ferdinandea Island, the 'Neverland' of the Sicily Channel (central Mediterranean Sea)

Daniele Spatola[a], Attilio Sulli[b], Luca Basilone[c], Daniele Casalbore[a,d], Simone Napoli[a], Gualtiero Basilone[e] and Francesco Latino Chiocci[a,d]

[a]Department of Earth Sciences, Sapienza University, Rome, Italy; [b]Department of Earth and Marine Sciences, University of Palermo, Palermo, Italy; [c]Instituto Oceanográfico da Universidade de São Paulo, Praça do Oceanográfico, São Paulo, Brazil; [d]Institute of Environmental Geology and Geo-Engineering, National Research Council, Rome, Italy; [e]Institute of Anthropic Impact and Sustainability in Marine Environment IAS – CNR, Consiglio Nazionale delle Ricerche – Torretta Granitola (TP), Granitola Torretta, Italy

ABSTRACT

We present the bathy-morphological map at a scale of 1: 50,000 of the area around the submerged Ferdinandea Island, the 'Neverland' of the Sicily Channel (central Mediterranean Sea). We investigate an area of 100 km^2, between 10 and 350 m, which is part of a triangular morphological high, 360 km^2 wide, representing the SE-wards prolongation of the Adventure Bank. The study is based on the morphometric analysis based on high resolution multibeam, and sub-bottom CHIRP profiles collected in 2015. The area around the remains of Ferdinandea Island is morphologically shaped by the interplay between volcanic, tectonic, fluid seepage, and oceanographic processes. Since the study area is considered a hot spot of biodiversity affected by maritime traffic (especially in Ferdinandea Channel) and hosting communication pipelines, this map provides insights both for habitat mapping purposes and preliminary marine geohazard assessment due to the occurrence of historically active submarine volcanoes, pockmarks, and mass transport deposits.

ARTICLE HISTORY
Received 8 February 2023
Revised 28 June 2023
Accepted 25 July 2023

KEYWORDS
Multibeam bathymetry; pockmark; submarine volcano; seismic reflection; Sicily Channel

1. Introduction

The Sicily Channel is a shallow marine sector between Sicily and Africa, characterised by a large and gently sloping (generally less than 1–2°) continental shelf (Figure 1). The shelf break is located at depths between ~ 100 m in the central part and ~ 150 m along the Adventure Bank and Ragusa Offshore (Todaro et al., 2021). The southern Sicilian coast with its several small touristic villages represents an important contribution to Italian tourism and to the economy of the island.

Since the Plio-Pleistocene, the Sicily Channel is characterised by both terrestrial and marine volcanic activity: the former ones is mainly concentrated in Pantelleria and Linosa Islands (Rotolo et al., 2006), whereas marine activity is mostly localised along the submarine banks such as Adventure Bank, Graham Bank, Nameless Bank, and many other minor submarine banks (Lodolo et al., 2012; Spatola et al., 2018a; 2018b), even if also the 1891 eruption of Pantelleria was submarine (Conte et al., 2014).

The Graham Bank is a small submarine volcanic region located in the upper slope of the north-western Sicily Channel (Figure 1), which was affected by numerous volcanic eruptions in the last 200 years (Calanchi et al., 1989), and where fluid escape phenomena (both cold and hydrothermal) controlled by faults (Figure 2(a)) are documented (Coltelli et al., 2016; Spatola et al., 2018a; 2018b). One the most well-known volcanic event (in the historical time) was in the 1831 when the emergence and rapid disappearance of the 'Ferdinandea Island' occurred (Calanchi et al., 1989; Colantoni et al., 1975; Washington, 1909). The recent acquisition of high resolution multibeam bathymetry data associated with high resolution acoustic profiles enhanced the knowledge of submarine volcanic areas all over Sicily Channel as well as the Graham Bank (Cavallaro & Coltelli, 2019; Civile et al., 2008; Coltelli et al., 2016; Spatola et al., 2017; 2018b).

In the last decades, great attention has been devoted to the characters of the flanks in active geologically areas such as active insular (Chiocci & De Alteriis, 2006) and in active/young submarine volcanoes (Camargo et al., 2019) because they can be a potential geohazard for infrastructures and surrounding coastal communities. In this regard, the study area is an important communication path, with intense ship

CONTACT Daniele Spatola daniele.spatola@uniroma1.it Department of Earth Sciences, Sapienza University, Rome, Italy
Supplemental map for this article is available online at https://doi.org/10.1080/17445647.2023.2243305.

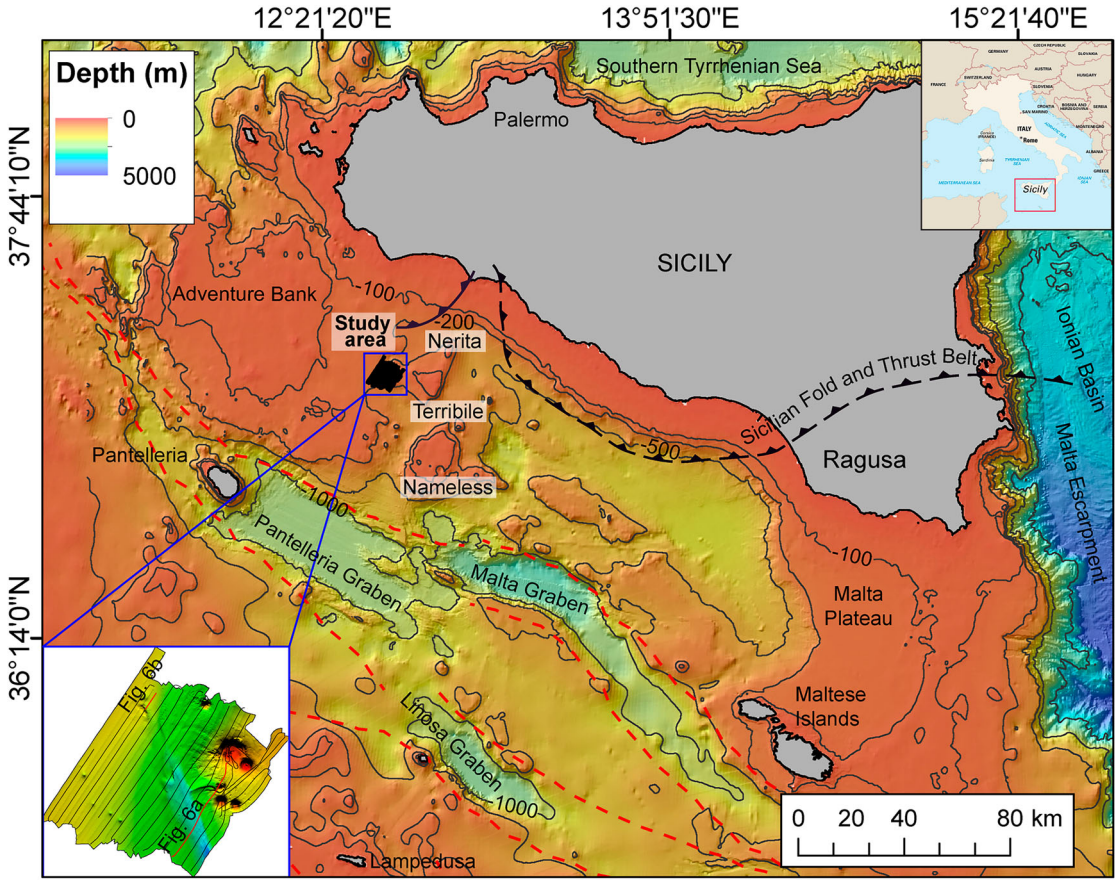

Figure 1. Location of the study area (blue box) and main physiographic features of the Sicily Channel (e.g. Plio-Pleistocene graben systems in red dashed lines). Background bathymetry from EMODnet bathymetry (http://www.emodnet-bathymetry.eu). In the lower left inset the spatial coverage of the high resolution multibeam data and sub-bottom CHIRP profiles (black lines).

transit and four pipelines connecting the minor islands and the Maltese archipelago (Figure 2(b)).

Recent studies demonstrated that volcanic banks represent, in the framework of the 'Sicily Channel Ecological or Biological Significant Area', unknown hot spots of biodiversity (Figure 2(c)) (Consoli et al., 2016; 2021; D'Elia et al., 2009) potentially threatened by human activities (Altobelli et al., 2017). They also have a great importance as main spawning area for important commercial fish species e.g. European Anchovy (*Engraulis encrasicolus*) (Basilone et al., 2020), and other species of high economic value of the commercial fishery (Altobelli et al., 2017). This is highlighted by the high maritime traffic especially during summer touristic season (Figure 2 (d)).

Considering the biological, geological, and economic importance of the area and nearby volcanic bank (Romagnoli et al., 2021), the aim of this study is to provide the first bathy-morphological map of the seafloor around the submerged remains of Ferdinandea Island at 1:50,000 scale, based on the morphometric analysis of the seafloor features using high resolution Digital Elevation Model (DEM). The map can be an important base tool for different issues, such as habitat mapping or first assessment of marine geohazard (Figure 2).

2. Materials and methods

2.1. Data

In this work, we used different types of high resolution geophysical data acquired during the ACUSCAL cruise (Inset in Figure 1), carried out in 2015 aboard the R/V Minerva1, in the framework of the RITMARE Project (CNR IAS Capo Granitola section).

(1) Multibeam echosounder coverage of ~ 100 km^2 of seafloor was obtained using the Reson SeaBat 7160, which generates 512 beams at a nominal frequency of 44 kHz. Positional data were provided by differential Global Positioning Systems (dGPS) by FUGRO SEASTAR. Bathymetric data were processed with PDS-2000 software, encompassing removal of erroneous beams, noise filtering, processing of navigation data, and correction for sound velocity. The final Digital Elevation Model (DEM) was obtained by gridding the soundings with a final cell size of 5 m. The DEM was exported as ASCII ESRI files to QGIS. ASCII ESRI files were transformed to raster files which were used to generate the main map as well as the figures in this paper. The multibeam data appears not correctly rollcalibrated or the sound velocity profile is not correct because it

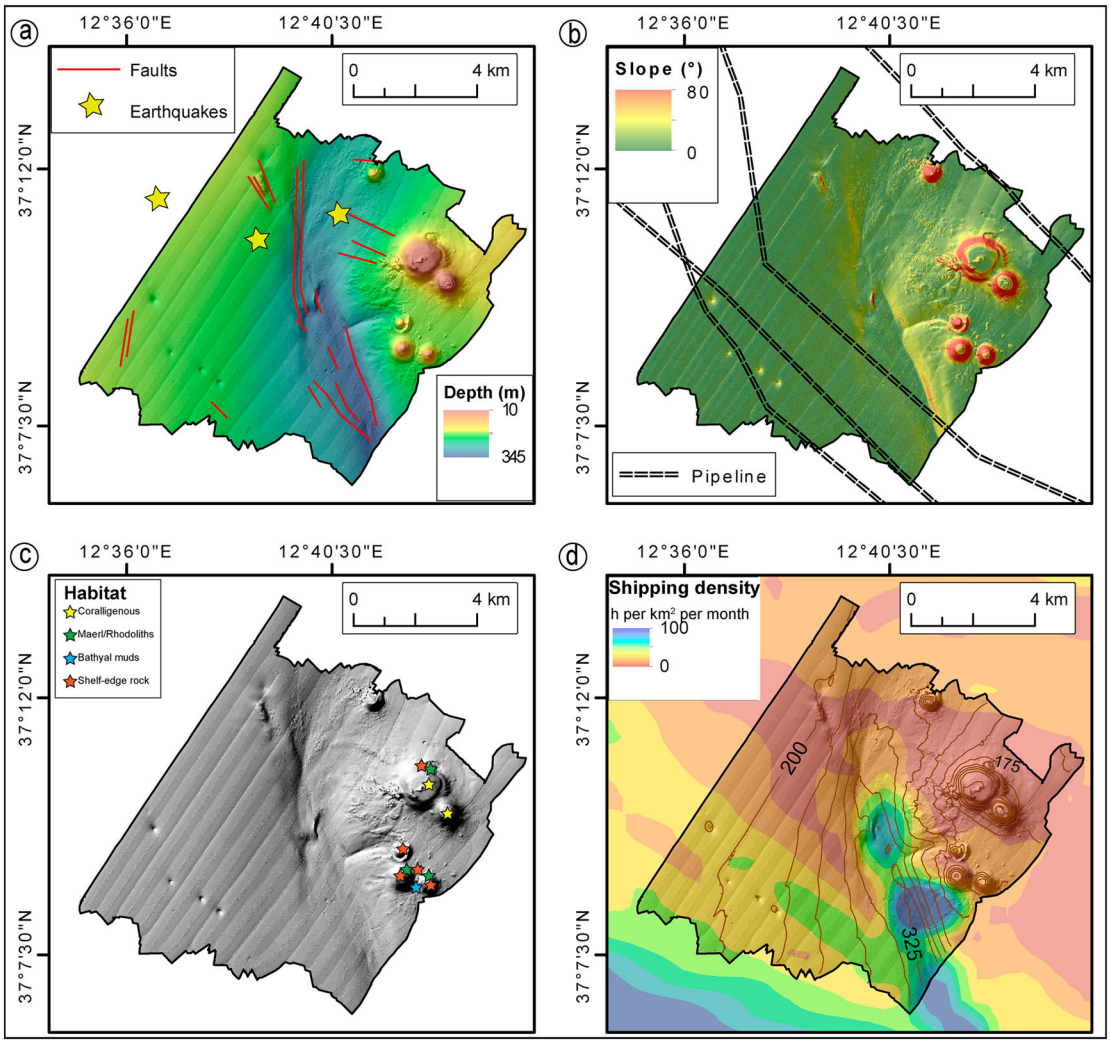

Figure 2. (a) Main faults (Spatola et al., 2018b) and earthquake epicentres recorded between 1981 and 2020 (http://iside.rm.ingv.it) overlaid on morpho-bathymetric map; (b) Distribution of pipelines (https://www.emodnet-humanactivities.eu) overlaid on slope map; (c) Distribution of the main habitats on shaded relief map (data from Consoli et al., 2021); (d) shipping density in the study area (interpolating data after https://www.emodnet-humanactivities.eu). Isobaths are drawn at 25 m intervals.

was acquired in very bad weather conditions. During the post-processing, we reduce the level of the noise to a minimum.

(2) A grid composed of 25 high resolution acoustic profiles (~ 200 km) was acquired using a hull-mounted 16 transducer Teledyne/Benthos CHIRP III profiler with frequencies ranging between 2 and 7 kHz, a ping rate between 250 and 750 ms, Tx power between 5 and 7, a pulse length of 10 ms and 30–42 db of gain. The profiles were processed and interpreted using Kingdom and GeoSuite Work software packages. Time-depth conversions of the sub-bottom CHIRP profiles have been made using the interval velocity described Spatola et al. (2018b).

2.2. Morphometric parameters

The morphometric characterisation of seafloor features was performed by using a semi-automatic method for extracting the main parameters according to the recent literature in submarine volcanic settings in the Tyrrhenian Sea (Sulli et al., 2020), in the Canary Islands (Ruiz et al., 2000), and in the Sicily Channel (Cavallaro & Coltelli, 2019; Spatola et al., 2018b) for an accurate morphological characterisation of the area. We used this morphometric approach to identify different family of seafloor morphologies (i.e. volcanic edifices and pockmarks) to be assessed. The integration of their morphological trends with geological, and geophysical data can be a good tool to better understand the volcano and pockmark evolution models in the area.

Volcanic edifices. The limit of the volcanic edifices was manually performed based on the sharp breaks in slope recognised in the cross-section profiles. The edifice limit is used to calculate both the enclosed basal surface and a number of linear parameters (e.g. major, minor and mean axis). We also measured the summit area as the area within the bathymetric contour above which slopes strongly decrease as they reach the summit, and the summit diameter as the

width of a circle with an area equal to that of the summit area (more detail in Grosse et al., 2012).

Finally, other parameters were calculated such as: (1) flatness (f = (ds / 2) / d), (2) diameter flank slope (fs = arctan (2 h / (D − d))), (3) ellipticity index (ei = (π*(Major Axis/2)^2)/Surface), (4) dissection index (di = (Perimeter/2*Surface)*($\sqrt{}$(Surface/π))), and (5) eccentricity (e = ($\sqrt{}$(Major Axis/2)^2-(Minor Axis/2)^2/ Major Axis/2)) (Grosse et al., 2009, 2012; Spatola et al., 2018). To estimate the volume of the volcanic edifices and lava field, we used the 'Cut and Fill' tool in ArcMap (http://www.esri.com/arcgis/). The bases of the features were identified by sharp breaks of slope in the cross-sectional profile using the high resolution multi-beam data.

Pockmarks. For each pockmark, we extracted the different morphometric parameters from the high resolution bathymetric data according to the recent literature (e.g. Chen et al., 2015): Mean water depth (m), Mean diameter (m), Perimeter (m), Surface (km^2), Surface (m^2), summit water depth (m), basal water depth (m), Deepness (m), Max slope (°), Mean slope (°), Long axis orientation (°). We also calculated some of the above-mentioned parameters.

3. Regional setting

The Sicily Channel (central Mediterranean Sea) is a foreland element of the Africa compressive margin resulted from the collision between Africa and Europe (Figure 1) (Catalano et al., 2000; Corti et al., 2006). Stratigraphically, Sicily Channel is made up of a ~ 7 km-thick Meso-Cenozoic carbonate platform, with igneous intercalations (mostly basalts), overlie by pelagic deposits (Jongsma et al., 1985; Osler & Algan, 1999), and then by 2–2.5 km of Miocene-Pliocene siliciclastic, evaporitic and limestone deposits (Todaro et al., 2021; 2022). The succession is finally covered by Quaternary pelagic deposits (Jongsma et al., 1985; Osler & Algan, 1999).

Structurally the Sicily Channel is mainly characterised by the presence of NW-SE-oriented sub-vertical Neogene-Quaternary normal faults which are part of the Sicily Channel Rift Zone (Agius et al., 2022). The rifting generated a thinning of the continental crust (5–18 km) since the Early Pliocene, enabling both the opening of three large elongate depressions known as Pantelleria, Malta and Linosa Grabens and widespread volcanism with the formation of subaerial and submarine volcanic morphologies (e.g. Pantelleria and Linosa volcanic Islands, Graham and Nameless Banks, Figure 1). The Sicily Channel is affected by seismic activity with $M_L < 3.5$ and hypocentres up to 20 km deep (Galea, 2007).

In the Sicily Channel, two main water masses interact: the superficial Modified Atlantic Water (MAW: 0–200 m), entering by the Adventure Bank and flowing eastward, and the deeper Levantine Intermediate Water (LIW: 200–400 m), which is saltier and flows westward (Lafuente et al., 2002; Millot, 1999). The MAW splits in two sub-currents: the Atlantic Ionian Stream (AIS) and the Atlantic Tunisian Stream (ATS). The AIS flows to the south of the Adventure Bank and proceeds south-eastward while the ATS flows along the African coasts; locally it forms loop currents such as the Adventure bank vortex, and the Maltese Channel Crest (Lermusiaux & Robinson, 2001).

4. Geomorphological map of the Graham Bank region

The study area is the westernmost part of a triangular morphological high, ~360 km^2 wide, comprising the Graham (−10 m), Nerita (−16 m), and Terrible (−20 m) Banks (Figure 1). We focus on the seafloor: (1) around the submerged remains of the 'Ferdinandea Island' and associated cones, (2) the N-S channel (Ferdinandea Channel) and (3) the plateau to its southwest (Figure 3). The study area covers a surface of ~100 km^2 between 10 and 350 m water depth. Both multibeam and CHIRP data allow to identify and map different morphological features, linked to different geological processes (i.e. volcanic, tectonic, oceanographic, mass-wasting, and fluid flow processes) that interact in shaping of the seafloor topography of the study area.

In the following section we divide the description of the area into two sectors showing marked differences in terms of morphology and related processes: (1) the eastern sector where the volcanic activity is the main agent and (2) the central/western sector where erosive-depositional, mass-wasting, oceanographic and tectonically-controlled fluid escape processes prevail.

4.1. Eastern sector

The eastern sector, due to its volcanic nature, has a rather rougher seafloor especially if compared to the neighbouring central/western part. It is characterised by the occurrence of scattered positive reliefs (e.g. isolated blocks, auxiliar cones) ranging in size from metres to sub-metre, which are visible in the multibeam data (Figures 3 and 4).

The most relevant seafloor features are six volcanic edifices with different shapes and sizes (V1-6 in Figure 4). These submarine volcanoes have mean axis ranging from ~ 0.5 and 2 km, heights from ~ 100 and 170 m, and areas from 0.2 and 3.2 km^2. All the measured morphometric parameters of the six volcanic edifices are tabulated in Table 1.

V1-6 mainly occur as isolated features apart from V2 and V3 that are partially coalescent at their base,

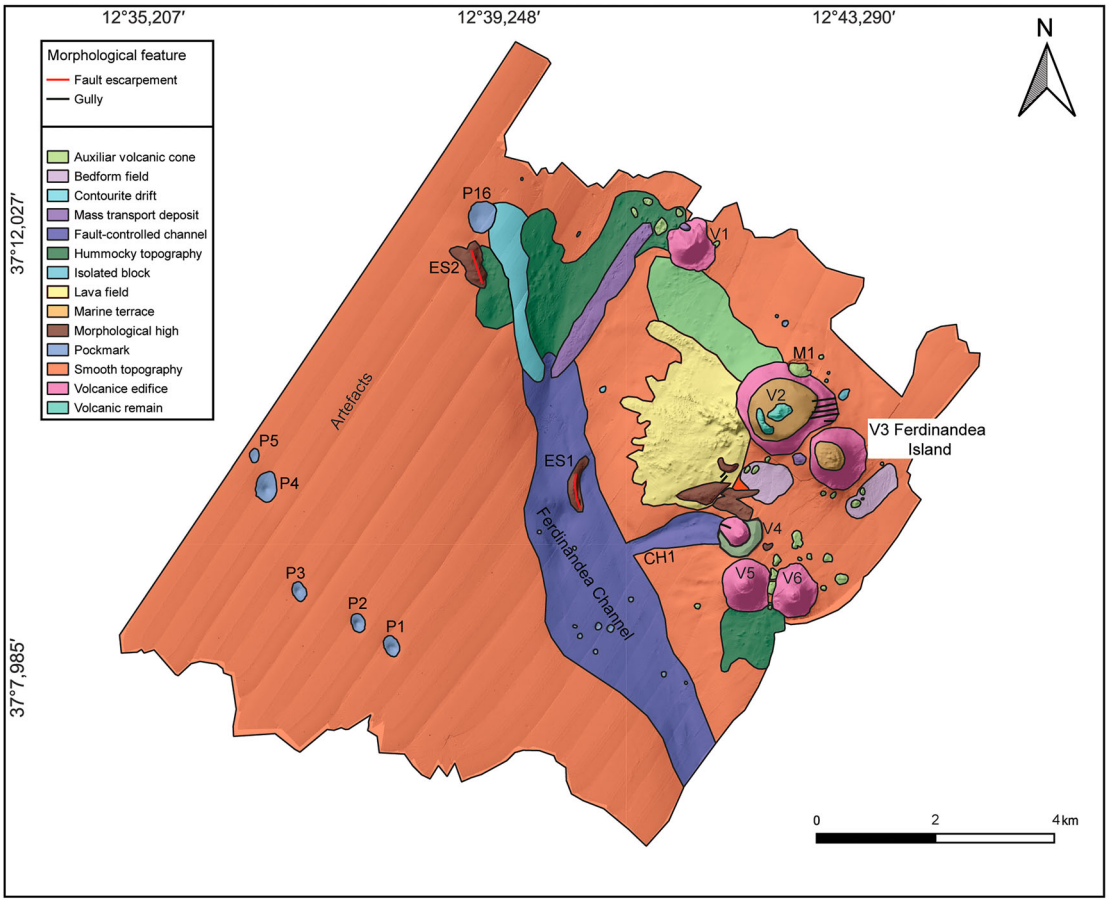

Figure 3. Bathy-morphologic map of the Graham Bank region draped over the shaded relief map of the seafloor, showing the main morphological features identified across the study area. ES: Escarpment; CH: Channel; P: Pockmark; M: Mound.

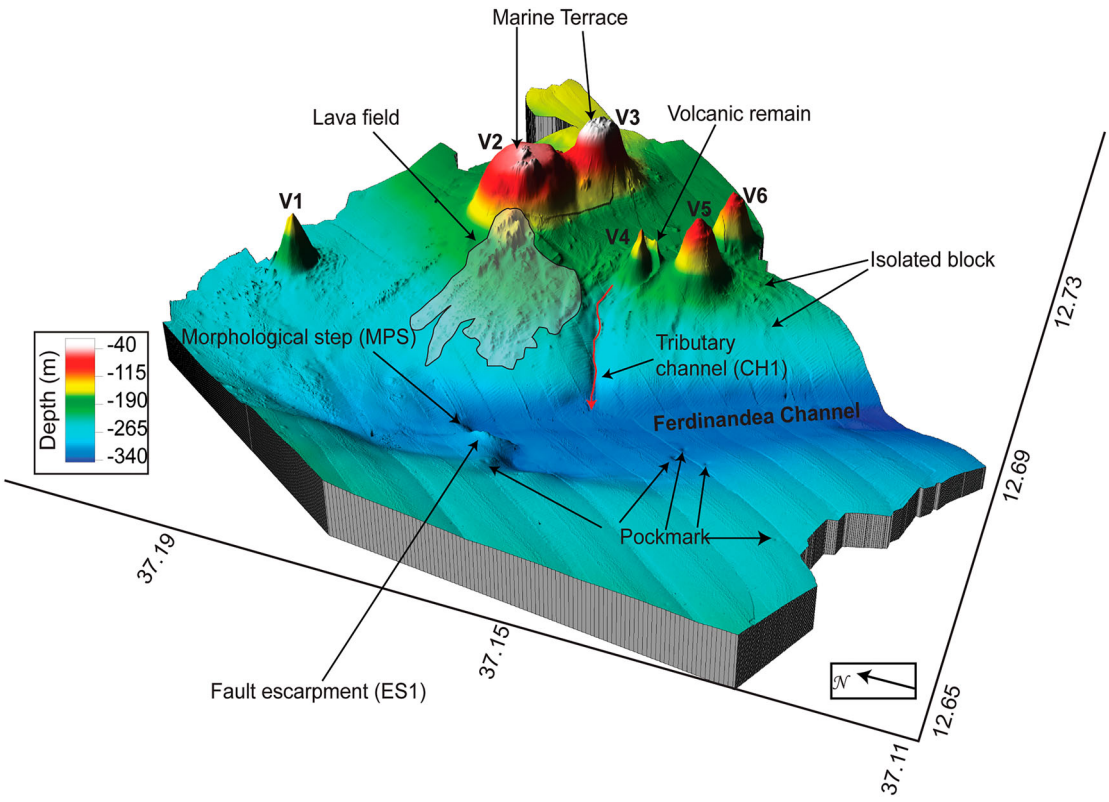

Figure 4. 3-D perspective view (vertical exaggeration 4×) of the study area, where the main volcanic, fluid flow and tectonic features are indicated.

Table 1. Measured/estimated morphometric parameters of volcanoes V1-6 (see 'Materials and methods' and Figure 4).

Volcanoes	Major axis (km)	Minor axis (km)	Mean axis (km)	Mean radius (km)	Base surface (Km^2)	Summit surface (Km^2)	Base perimeter (Km)	Summit perimeter (km)	Volume (km^3)	Height (m)	Summit depth (m)	Base depth (m)	Basal ratio (bsr)	Height/ Mean radius	Height/ Mean axis	Summit mean axis (m)	Summit mean axis/ Mean axis	Flatness	Flank slope (°)	Ellipticity index	Dissection index	Height/ Base surface	Eccentricity
V1	0.705	0.580	0.643	0.321	0.291	0.004	2.081	0.268	0.012	108	122	230	0.823	0.336	0.168	75	0.117	0.065	1.565	1.341	1.089	0.371	0.5685
V2	2.178	1.801	1.990	0.995	3.147	0.817	7.059	3.251	0.572	171	33	204	0.827	0.172	0.086	1039	0.522	0.288	1.567	1.183	1.123	0.054	0.5623
V3	0.995	0.985	0.990	0.495	0.737	0.175	3.228	1.505	0.136	130	10	140	0.990	0.263	0.131	486	0.491	0.247	1.567	1.055	1.061	0.176	0.1414
V4	0.545	0.514	0.530	0.265	0.206	0.002	1.654	0.164	0.043	124	108	232	0.943	0.468	0.234	52	0.098	0.051	1.567	1.132	1.028	0.602	0.3325
V5	0.770	0.720	0.745	0.373	0.438	0.017	2.413	0.474	0.098	115	77	192	0.935	0.309	0.154	150	0.201	0.104	1.566	1.064	1.029	0.263	0.3545
V6	1.065	0.935	1.000	0.500	0.715	0.008	3.081	0.339	0.167	139	70	209	0.878	0.278	0.139	121	0.121	0.065	1.567	1.245	1.028	0.194	0.4788
Minimum	0.545	0.514	0.530	0.265	0.206	0.002	1.654	0.164	0.012	108	10	140	0.823	0.172	0.086	52	0.098	0.051	1.565	1.055	1.028	0.054	0.141
Maximum	2.178	1.801	1.990	0.995	3.147	0.817	7.059	3.251	0.572	171	122	232	0.990	0.468	0.234	1039	0.522	0.288	1.567	1.341	1.123	0.602	0.568
Mean	1.043	0.923	0.983	0.491	0.922	0.171	3.253	1.000	0.171	131	70	201	0.899	0.304	0.152	321	0.258	0.137	1.566	1.170	1.060	0.277	0.406
Standard deviation	0.588	0.469	0.528	0.264	1.111	0.324	1.957	1.206	0.205	22	43	34	0.068	0.098	0.049	386	0.196	0.104	0.001	0.111	0.039	0.190	0.164

forming a complex edifice oriented ~ NW-SE knew in literature as Graham Bank. The six volcanic cones generally have circular base (bsr with average of 0.89 in Table 1), only in few cases elliptical or irregular, as also highlighted by the relationship between the dissection index and ellipticity index (Figure 5(a)). A negative correlation between heights of V1-6 and water depth (Figure 5(d)) suggests a possible influence of hydrostatic pressure on magma properties, eruption style and deposit characteristics (Cas & Simmons, 2018).

V1 is a small volcanic edifice ~ 110 m high and up to 700 m wide at the bottom and 75 m at the top. It rises from a smooth topography at 230 m depth and is bounded by strong step flanks up to 26°, locally characterised by a small mass transport deposit (Figure 3). This MTD appears in the CHIRP profile as an isolated body with an irregular shape composed by acoustic transparent/chaotic facies (more detail in Spatola et al., 2018b).

Scatter plots in Figure 5(b,c) show that the volcanic edifices can be divided in two main groups: (1) conical shape with a flatness value lower than 0.15 (V1,4,5,6) and (2) flat-topped shape with higher values of flatness (V2-3). The flat-topped features of the bigger V2, and the minor V3 (Ferdinandea Island) are located in the shallowest part of the study area (Figures 3 and 4), with their summit lying at 10 and 33 m water depths (Figure 5(c)). We interpret their flat surfaces as marine terraces formed by wave erosion during the subaerial phases such as the emergence and disappearance of the 'Ferdinandea Island' (Colantoni et al., 1975). They show very steep flanks (up to 27°) incised by small gullies and slide-scars.

Along the southwestern flank of V2, the seafloor is characterised by complex lava field flowing downslope (Figures 3 and 4), which is ~ 2.2 km long and has an estimated volume of 0.017 km^3. The northern flank of V2 is characterised by a NW-SE elliptical depression (~ 500 m long) bounded by steep walls (up to 20°) from few metres to 10 m high. The depression internally is characterised by the occurrence of a mound up to 13 m high and 160 m wide (M1 in Figure 3). Considering the volcanic context as well as the curvilinear shape of the above mentioned depression, we suggest that its formation is linked to the presence of active hydrothermal vents detected as hydroacoustic anomalies in the water column by sub-bottom CHIRP profiles (Figure 6(a)) (Coltelli et al., 2016; Spatola et al., 2018b).

The smaller V4 has a more complex configuration that suggests a multi-stage construction mechanism. It is conical-shaped, 650 m wide, 100 m high, and covers a surface of 0.16 km^2 at water depth ranging from ~ 108 to 205 m (Figures 3 and 4). Its flanks have steep slope gradients of up to 28° in the eastern flank, decreasing to 15° in the western flank. The

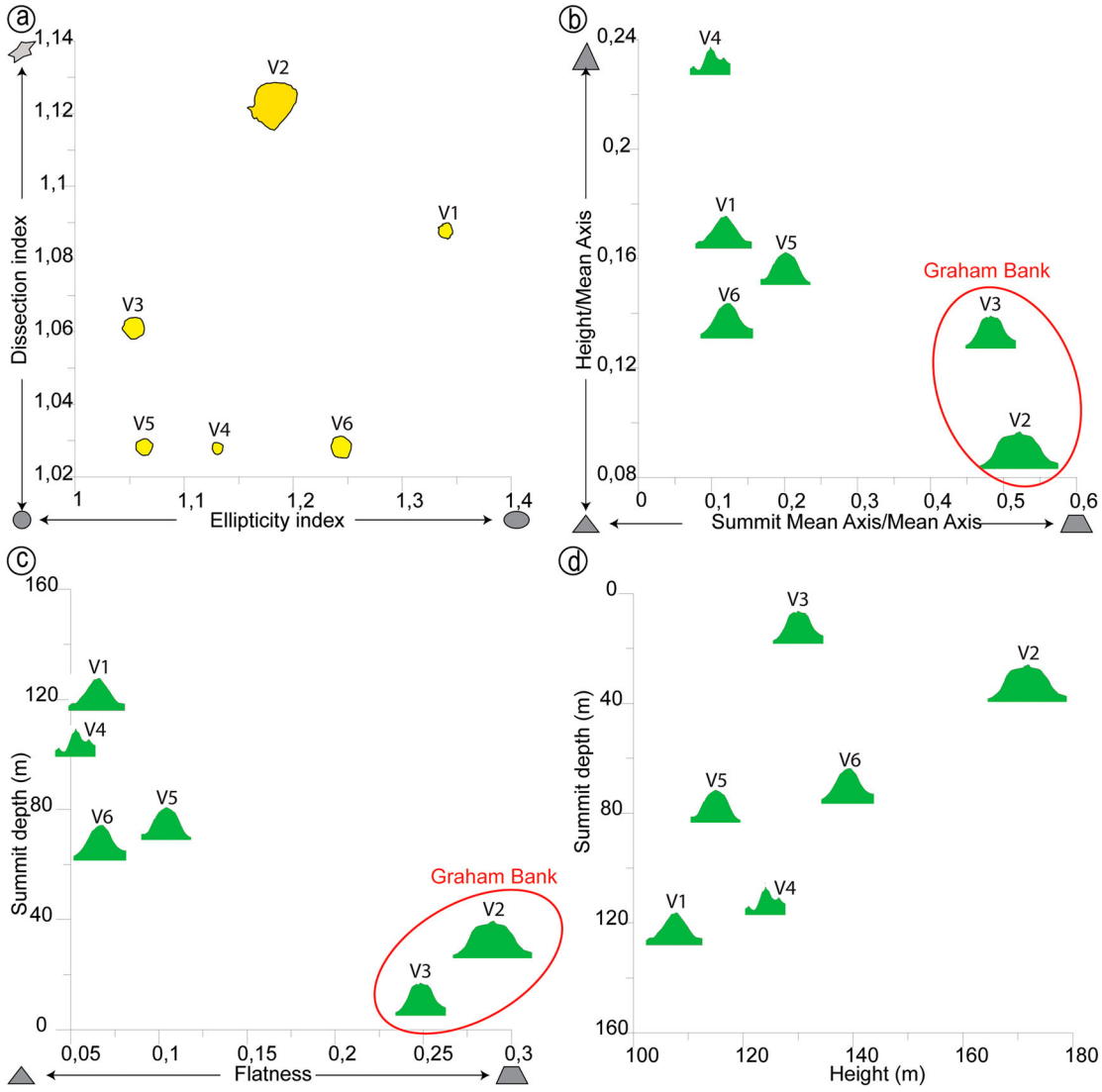

Figure 5. Scatter plots of (a) Dissection index versus Ellipticity index of V1-6 illustrating plan shape variations; (b) Height/Mean Axis versus Summit Mean Axis/Mean Axis of V1-6, illustrating varying profile shapes; (c) Summit Water Depth versus Flatness; (d) Summit Water Depth versus Height.

bathymetric data likely shows in the southern flank of V4 the presence of a saddle ~ 20 m deep and ~ 15° steep, with U-shape in cross-section bordered by an annular ridge interpretable as the remains of an older and larger volcanic edifice (Figures 3 and 4).

V5 is a volcano 115 m high and 770 m wide. It rises from a gentle sloping seafloor at ~ 190 m depth and is bordered by strong inclined flanks with 22° of average slope. It is rimmed on the top by a small plain surface of about 150 m wide with a slope of 8°.

V6 is a volcano 139 m high and 1 km wide at the bottom and ~ 121 m at the top. It rises from a sloping seafloor at 210 m depth and is bordered by very steep flanks with slopes of about 25°.

4.2. Central/Western sector

The central sector is dominated by an asymmetric channel, that we named 'Ferdinandea Channel', covering an area of ~ 12 km^2 wide and crossing the whole investigated area (Figures 3 and 4). The Ferdinandea Channel is a fault-controlled morphology (Spatola et al., 2018b), oriented NW-SE, up to 1.5 km wide and more than 10 km long (according to the EMODnet Bathymetry). The water depth ranges from 200 m at the head to 350 m at southern end in the study area. Its cross-sectional profile is asymmetric with walls from 30 to 80 m high with slope gradients from 3 to 7°.

The longitudinal profile of the Ferdinandea Channel is almost linear interrupted by a morphological step in the central part forming a break of slope up to 20 m high (MPS Figure 4). The western wall of the Ferdinandea Channel is also marked by the occurrence of a NW-SE fault escarpment, ~ 650 m long forming a relief of ~ 30 m (ES1 in Figures 3 and 4).

The seafloor in the Ferdinandea Channel is characterised by smooth morpho-acoustic facies, and it

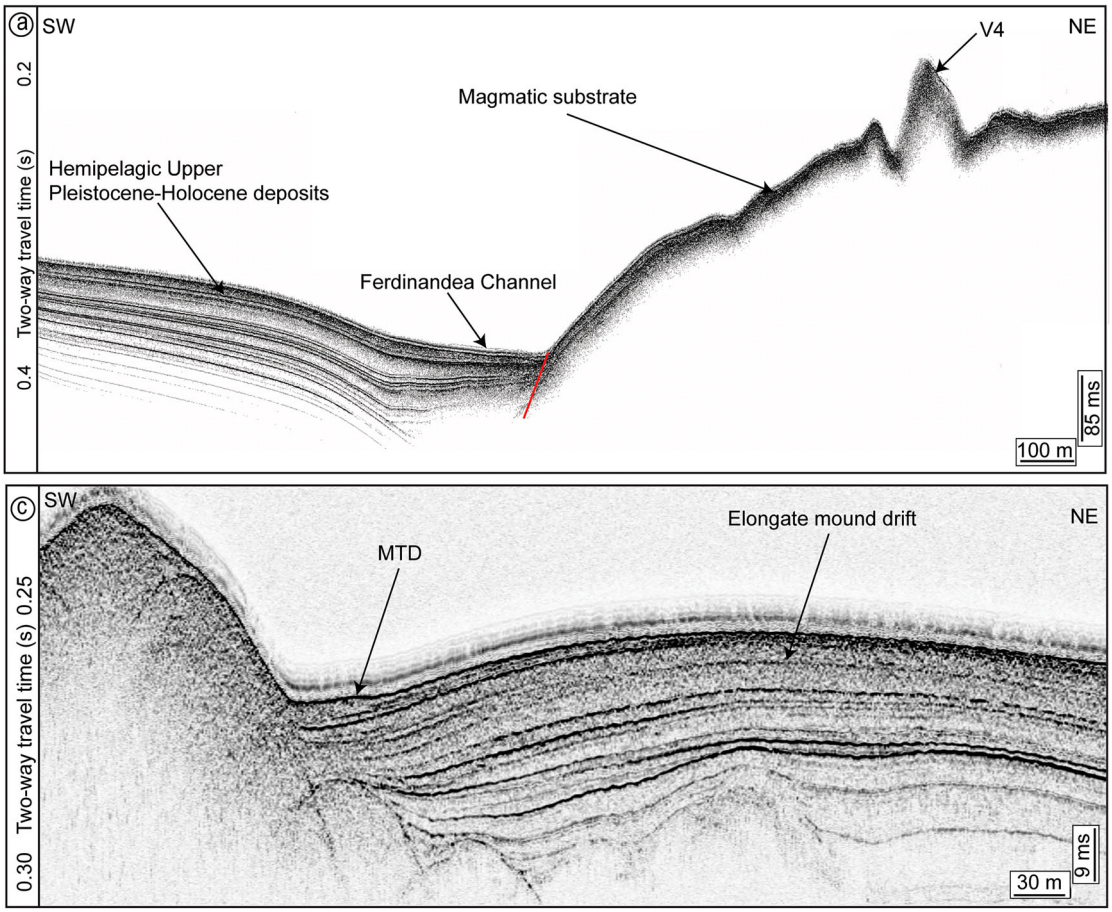

Figure 6. (A) Sub-bottom CHIRP profile acquired on the central/eastern part of the study area showing the main features of the area, such as hemipelagic deposits on the western plateau, the asymmetric Ferdinandea Channel, and the volcanic edifice V4. (B) Zoom of a Sub-bottom CHIRP profile showing the chaotic acoustic facies of a MTD and the mounded internal geometry of the Elongate mound drift. Location in Figures 1 and 3.

receives a tributary channel (CH1 in Figure 4) originating from V4 edifice. CH1 is ~ 1.5 km long, up to 250 m wide and has a U-shaped cross-section. In the central part, the seafloor of Ferdinandea Channel is locally punctuated by 10 sub-circular pockmarks with axis between ~ 45 and 130 m and depths between 2 and ~ 12 m (Figures 3 and 4). They are predominantly V-shaped in cross-section and organised either as isolated, clustered, or only in few cases aligned along a NW-SE trend.

Six bigger sub-circular pockmarks (P1-5, 16) with axis up to 540 m, and depths up to 22 m (Figure 3 and Table 2) are recognised at the seafloor of the western sector, which displays a flat morphology (slope gradient between 1.2 and 1.5°). The CHIRP profile shows the occurrence of a very smooth morpho-acoustic (Figure 3) due to the presence of hemipelagic Upper Pleistocene-Holocene deposits making up the uppermost part of the subsurface (Figure 6(a)). These negative features are very similar in size and shapes to the pockmarks documented all over the Sicily Channel (Micallef et al., 2019). We classified the fluid flow negative features in normal and giant pockmarks (Table 2), on the basis of their parameters (i.e. size and depth), according to the recent nomenclature (Hovland et al., 2002; Judd & Hovland, 2007).

As for as morphometry of pockmarks is concerned, normal pockmarks are more circular than giant pockmarks (except P16) that are marked by high ellipticity values (Figure 7(a,b)), and high axis ratio values (Table 2). This morphological character is also confirmed by the scatter plots b that relates the depth of the pockmarks with their eccentricity. Their eccentricity is probably influenced by the loop currents (Lermusiaux & Robinson, 2001) forming the elongated mound drift recognised by Spatola et al. (2018b) and the bedform fields described by Cavallaro and Coltelli (2019) around the Graham Bank (Figure 3). The elongate mound drift that shows high similarity with the contourite drift deposits documented in the south-central Mediterranean Sea (Micallef et al., 2019; Spatola et al., 2021). It consists of an internal aggradational stacking pattern with mounded packages of continuous, moderate to high amplitude seismic reflectors, and is internally composed by a mix of hemipelagic Upper Pleistocene-Holocene deposits (Figure 6(b)).

In the study area, pockmarks tend to be larger where they are less dense, smaller where they are denser as in the UK sector of the North Sea. Scatter plots c

Table 2. Measured/computed morphometric parameters of Pockmarks P1-17 (see 'Materials and methods' and Figure 3).

Pockmarks	Major axis (m)	Minor axis (m)	Mean axis (m)	Mean radius (m)	Axis ratio	Deepness (m)	Surface (m^2)	Perimeter (m)	Summit depth (m)	Basal depth (m)	Depth/ Radius	Flank slope (°)	Ellipticity index	Dissection index	Depth/ Surface	Eccentricity	Morphological type
P1	370	242	306	153	1.53	14	70933	1016	221	235	0.09	1.516	1.5158	1.0764	0.0002	0.7564	Giant
P2	320	220	270	135	1.45	15	58813	918	213	228	0.11	1.522	1.3675	1.0681	0.0003	0.7262	Giant
P3	325	225	275	138	1.44	22	59083	925	202	224	0.16	1.538	1.4041	1.0738	0.0004	0.7216	Giant
P4	520	356	438	219	1.46	18	143939	1448	196	214	0.08	1.530	1.4754	1.0769	0.0001	0.7289	Giant
P5	240	161	201	100	1.49	3	29378	652	192	195	0.03	1.327	1.5399	1.0734	0.0001	0.7416	Normal
P6	86	84	85	43	1.02	2	5436	270	323	325	0.05	1.320	1.0686	1.0333	0.0004	0.2144	Normal
P7	72	56	64	32	1.29	2	3274	228	311	313	0.06	1.260	1.2436	1.1243	0.0006	0.6285	Normal
P8	69	67	68	34	1.03	6	3502	217	278	284	0.18	1.485	1.0678	1.0347	0.0017	0.2390	Normal
P9	127	112	120	60	1.13	5	11874	401	313	318	0.08	1.458	1.0668	1.0384	0.0004	0.4715	Normal
P10	125	106	116	58	1.18	5	10273	376	309	314	0.09	1.453	1.1946	1.0468	0.0005	0.5300	Normal
P11	69	49	59	30	1.41	4	3041	206	297	301	0.14	1.397	1.2296	1.0541	0.0013	0.7041	Normal
P12	90	79	85	42	1.14	5	5690	283	297	302	0.12	1.457	1.1181	1.0586	0.0009	0.4791	Normal
P13	82	80	81	41	1.03	3	5058	267	301	304	0.07	1.402	1.0441	1.0593	0.0006	0.2195	Normal
P14	90	78	84	42	1.15	4	6181	290	326	330	0.10	1.428	1.0292	1.0408	0.0006	0.4989	Normal
P15	53	45	49	25	1.18	12	1903	160	310	322	0.49	1.522	1.1593	1.0349	0.0063	0.5283	Normal
P16	540	440	490	245	1.23	13	194404	1634	198	211	0.05	1.524	1.1781	1.0457	0.0001	0.5797	Giant
P17	115	93	104	52	1.24	8	8179	335	202	210	0.15	1.494	1.2699	1.0452	0.0010	0.5882	Normal

Pockmarks	Major axis (m)	Minor axis (m)	Mean axis (m)	Mean radius (m)	Axis ratio	Depth (m)	Surface (m^2)	Perimeter (m)	Summit depth (m)	Basal depth (m)	Depth/ Radius	Flank slope (°)	Ellipticity index	Dissection index	Depth/ Surface	Eccentricity
Minimum	53	45	49	25	1.02	2	1903	160	192	195	0.03	1.26	1.0292	1.0333	0.0001	0.2144
Maximum	540	440	490	245	1.53	22	194404	1634	326	330	0.49	1.54	1.5399	1.1243	0.0063	0.7564
Mean	194	147	170	85	1.26	8	36527	566	264	272	0.12	1.45	1.2337	1.0579	0.0009	0.5503
Standard deviation	162	114	138	69	0.17	6	55424	458	54	50	0.10	0.08	0.1703	0.0231	0.0015	0.1833

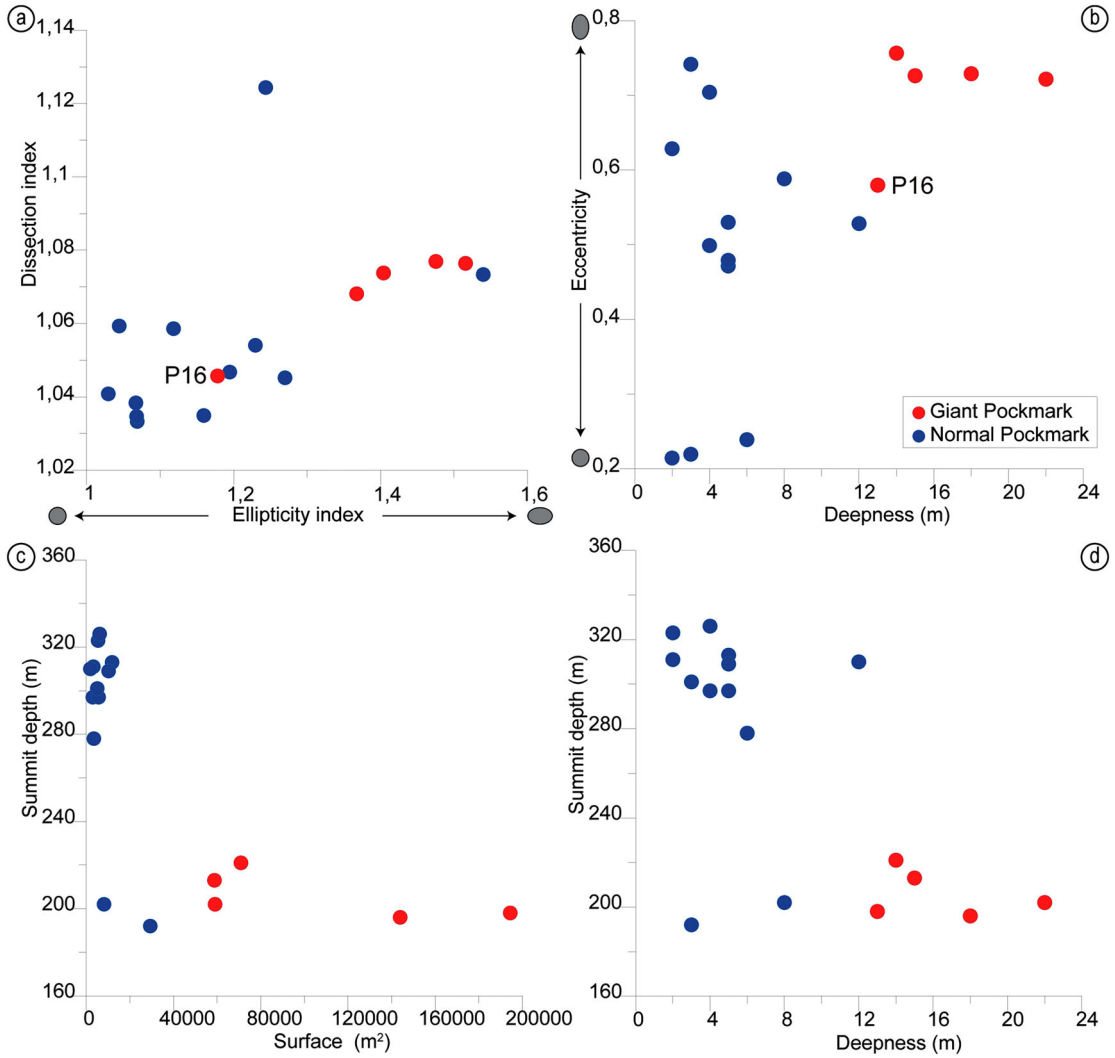

Figure 7. Scatter plots of pockmarks morphometric parameters. (a) Dissection index versus Ellipticity index; (b) Eccentricity versus Pockmark Deepness; (c) Summit Water Depth versus Surface; (d) Summit Water Depth versus Pockmark Deepness. Red dots indicate giant pockmarks and blue dots the normal pockmarks.

and d in Figure 7 show that the normal pockmarks are mainly localised in the deepest part of the study area. The presence of giant pockmarks at shallower depths could be related to the texture of the sediments (Ellis et al., 1986; Uchupi et al., 1996) or to the thickness of the 'pockmarkable' sediment (or both) as evidenced by the presence of Late Pleistocene-Holocene hemipelagic deposits (Figure 6). On the other hand, normal pockmarks in the Ferdinandea Channel are well matched with coarser grain size and cyclical fluid emissions (Hovland et al., 2002) through subvertical normal faults with seafloor morphological expression (e.g. ES1 in Figures 3 and 4) (Spatola et al., 2018b). Evidence of recent tectonics is recognised in the north-western part as small quasi-linear escarpment-oriented NW-SE up to 700 m in length and up to 35 m high (ES2 in Figure 3). Finally, mass transport deposits with irregular blocky topography, related to gravity-driven mass flows, are documented across the study area (Figure 6(b)).

5. Conclusions

The main outcome of this paper is the morphological map at a scale of 1:50,000 that better defines the geological character of area around the submerged remains of the Ferdinandea Island, the 'neverland' of the Sicily Channel (central Mediterranean Sea). It provides insights for habitat mapping since the study area is an important hot spot of biodiversity especially for the spawning of different fish species (e.g. European Anchovy (*Engraulis encrasicolus*)).

The study area shows marked morphological difference between the eastern sector controlled mainly by volcanic activity and the central/western sector where sedimentary factors (such as oceanography, mass-wasting, and fluid flow processes) dominate. The eastern sector is characterised by the occurrence of four conical volcanic cones (V1-4,5,6) and two flat-topped volcanic cones V2-3 (Graham Bank) with at their top large marine terraces formed by wave

erosion. The central/western sector is dominated by the 'Ferdinandea Channel' and is locally punctuated by seventeen normal and giant pockmarks and mass transport deposits.

In conclusion, in view of the biological, geological, and economic importance of the study area, the map represents an important base tool for different scientific studies such as for the geomorphological and habitat mapping or for the marine geohazard assessment especially considering the high maritime traffic and the occurrence of communication pipelines in the area.

Software

PDS2000 was used to process multibeam data and to generate the marine DTM, while Global Mapper was used to visualise data using shaded relief maps, contour maps and slope gradient maps to perform morphological analyses and extract morphological features from the DTM. The design of the final map presented in this work was produced using QGIS and ArcGIS with additional refinement using the open source Inkscape software.

Acknowledgements

Multibeam bathymetry was acquired during a cruise carried out by a team from Consiglio Nazionale delle Ricerche - (IAS-CNR) Torretta Granitola (TP) – Italy in the framework of the 'RITMARE' project. We are grateful to all the crew of R/V Minerva1 for their skilled help during data acquisition and onboard operations. All participants and technical staff from the IAS-CNR are gratefully acknowledged for their contribution to the research work. We thank Francesca Budillon, Claudia Romagnoli and Thomas Pingel for their constructive comments.

Disclosure statement

No potential conflict of interest was reported by the author(s).

Funding

This study benefited from funding and ship-time through the RITMARE project (CNR Mazara del Vallo, Capo Granitola section). D.S. is founded by PON – 'Research and Innovation' 2014–2020.

Data availability statement

The Department of Earth and Marine Sciences of the University of Palermo, for institutional purposes, so their access will be available by contacting the reference person (attilio.sulli@unipa.it) upon reasonable request.

References

Agius, M. R., Magrini, F., Diaferia, G., Kästle, E. D., Cammarano, F., Faccenna, C., Funiciello, F., & van der Meijde, M. (2022). Shear-velocity structure and dynamics beneath the Sicily channel and surrounding regions of the central Mediterranean inferred from seismic surface waves. *Geochemistry, Geophysics, Geosystems*, *23*(10), e2022GC010394. https://doi.org/10.1029/2022GC010394

Altobelli, C., Perzia, P., Falautano, M., Consoli, P., Canese, S., Romeo, T., & Andaloro, F. (2017). Mediterranean banks in EBSA area: Hotspots of biodiversity under threat. *Marine Environmental Research*, *131*, 57–68. https://doi.org/10.1016/j.marenvres.2017.09.005

Basilone, G., Ferreri, R., Barra, M., Bonanno, A., Pulizzi, M., Gargano, A., Fontana, I., Giacalone, G., Rumolo, P., & Mazzola, S. (2020). Spawning ecology of the European anchovy (Engraulis encrasicolus) in the Strait of Sicily: Linking variations of zooplankton prey, fish density, growth, and reproduction in an upwelling system. *Progress in Oceanography*, *184*, 102330. https://doi.org/10.1016/j.pocean.2020.102330

Calanchi, N., Colantoni, P., Rossi, P. L., Saitta, M., & Serri, G. (1989). The Strait of Sicily continental rift systems: Physiography and petrochemistry of the submarine volcanic centres. *Marine Geology*, *87*(1), 55–83. https://doi.org/10.1016/0025-3227(89)90145-X

Camargo, J. M., Silva, M. V., Ferreira Júnior, A. V., & Araújo, T. C. (2019). Marine geohazards: A bibliometric-based review. *Geosciences*, *9*(2), 100. https://doi.org/10.3390/geosciences9020100

Cas, R. A., & Simmons, J. M. J. F. I. E. S. (2018). Why deep-water eruptions are so different from subaerial eruptions. *6*, 198.

Catalano, R., Franchino, A., Merlini, S., & Sulli, A. (2000). Central western Sicily structural setting interpreted from seismic reflection profiles. *Memorie Della Società Geologica Italiana*, *55*, 5–16.

Cavallaro, D., & Coltelli, M. (2019). The Graham volcanic field offshore southwestern Sicily (Italy) revealed by high-resolution seafloor mapping and ROV images. *Frontiers in Earth Science*, *7*, 311. https://doi.org/10.3389/feart.2019.00311

Chen, J., Song, H., Guan, Y., Yang, S., Pinheiro, L. M., Bai, Y., Liu, B., & Geng, M. (2015). Morphologies, classification and genesis of pockmarks, mud volcanoes and associated fluid escape features in the northern Zhongjiannan Basin, South China Sea.

Chiocci, F. L., & De Alteriis, G. (2006). The Ischia debris avalanche: First clear submarine evidence in the Mediterranean of a volcanic island prehistorical collapse. *Terra Nova*, *18*(3), 202–209. https://doi.org/10.1111/j.1365-3121.2006.00680.x

Civile, D., Lodolo, E., Tortorici, L., Lanzafame, G., & Brancolini, G. (2008). Relationships between magmatism and tectonics in a continental rift: The Pantelleria Island region (Sicily Channel, Italy). *Marine Geology*, *251*(1-2), 32–46. https://doi.org/10.1016/j.margeo.2008.01.009

Colantoni, C. S., Levesque, T. J., & Ordeshook, P. C. (1975). Campaign resource allocations under the Electoral College. *The American Political Science Review*, *69*(1), 141–154.

Coltelli, M., Cavallaro, D., D'Anna, G., D'Alessandro, A., Grassa, F., Mangano, G., Patanè, D., & Gresta, S. (2016). Exploring the submarine graham bank in the sicily channel. *Annals of Geophysics*, *59*(2). S0208.

Consoli, P., Altobelli, C., Perzia, P., Bo, M., Rosso, A., Alongi, G., Serio, D., Canese, S., Romeo, T., & Andaloro, F. J. (2021). Species and habitats of conservation interest in the ecologically and biologically

significant area of the strait of Sicily: A contribution towards the creation of a specially protected areas of Mediterranean importance. *Mediterranean Marine Science*, *22*(2), 297–316. https://doi.org/10.12681/mms.25125

Consoli, P., Esposito, V., Battaglia, P., Altobelli, C., Perzia, P., Romeo, T., Canese, S., & Andaloro, F. (2016). Fish distribution and habitat complexity on banks of the Strait of Sicily (Central Mediterranean Sea) from remotely-operated vehicle (ROV) explorations. *PLoS One*, *11*(12), e0167809. https://doi.org/10.1371/journal.pone.0167809

Conte, A., Martorelli, E., Calarco, M., Sposato, A., Perinelli, C., Coltelli, M., & Chiocci, F. J. (2014). The 1891 submarine eruption offshore Pantelleria Island (Sicily Channel, Italy): Identification of the vent and characterization of products and eruptive style. *Geochemistry, Geophysics, Geosystems*, *15*(6), 2555–2574. https://doi.org/10.1002/2014GC005238

Corti, G., Cuffaro, M., Doglioni, C., Innocenti, F., & Manetti, P. (2006). Coexisting geodynamic processes in the Sicily Channel. *Special Papers-Geological Society of America*, *409*, 83. https://doi.org/10.1130/2006.2409(05)

D'Elia, M., Patti, B., Sulli, A., Tranchida, G., Bonanno, A., Basilone, G., Giacalone, G., Fontana, I., Genovese, S., & Guisande, C. (2009). Distribution and spatial structure of pelagic fish schools in relation to the nature of the seabed in the Sicily Straits (Central Mediterranean). *Marine Ecology*, *30*, 151–160. https://doi.org/10.1111/j.1439-0485.2009.00328.x

Ellis, J. P., McGuinness, W. T., & Ruud, S. (1986). Pockmarks of the northwestern Arabian Gulf, Oceanology: Proceedings of an international conference. *OnePetro*.

Galea, P. (2007). Seismic history of the Maltese islands and considerations on seismic risk. *Annals of Geophysics*, *50*, 725–740.

Grosse, P., van Wyk de Vries, B., Euillades, P. A., Kervyn, M., & Petrinovic, I. A. (2012). Systematic morphometric characterization of volcanic edifices using digital elevation models. *Geomorphology*, *136*(1), 114–131. https://doi.org/10.1016/j.geomorph.2011.06.001

Grosse, P., van Wyk de Vries, B., Petrinovic, I. A., Euillades, P. A., & Alvarado, G. E. (2009). Morphometry and evolution of arc volcanoes. *Geology*, *37*(7), 651–654. https://doi.org/10.1130/G25734A.1

Hovland, M., Gardner, J. V., & Judd, A. G. (2002). The significance of pockmarks to understanding fluid flow processes and geohazards. *Geofluids*, *2*(2), 127–136. https://doi.org/10.1046/j.1468-8123.2002.00028.x

Jongsma, D., van Hinte, J. E., & Woodside, J. M. (1985). Geologic structure and neotectonics of the North African Continental Margin south of Sicily. *Marine and Petroleum Geology*, *2*(2), 156–179. https://doi.org/10.1016/0264-8172(85)90005-4

Judd, A., & Hovland, M. (2007). *Seabed fluid flow: The impact on geology, biology and the marine environment*. Cambridge University Press.

Lafuente, J. G., García, A., Mazzola, S., Quintanilla, L., Delgado, J., Cuttita, A., & Patti, B. (2002). Hydrographic phenomena influencing early life stages of the Sicilian Channel anchovy. *Fisheries Oceanography*, *11*(1), 31–44. https://doi.org/10.1046/j.1365-2419.2002.00186.x

Lermusiaux, P. F. J., & Robinson, A. R. (2001). Features of dominant mesoscale variability, circulation patterns and dynamics in the Strait of Sicily. *Deep Sea Research Part I: Oceanographic Research Papers*, *48*(9), 1953–1997. https://doi.org/10.1016/S0967-0637(00)00114-X

Lodolo, E., Civile, D., Zanolla, C., & Geletti, R. (2012). Magnetic signature of the Sicily Channel volcanism. *Marine Geophysical Research*, *33*(1), 33–44. https://doi.org/10.1007/s11001-011-9144-y

Micallef, A., Spatola, D., Caracausi, A., Italiano, F., Barreca, G., D'Amico, S., Petronio, L., Coren, F., Facchin, L., Blanos, R., Pavan, A., Paganini, P., & Taviani, M. (2019). Active degassing across the Maltese Islands (Mediterranean Sea) and implications for its neotectonics. *Marine and Petroleum Geology*, *104*, 361–374.

Millot, C. (1999). Circulation in the Western Mediterranean Sea. *Journal of Marine Systems*, *20*(1–4), 423–442. https://doi.org/10.1016/S0924-7963(98)00078-5

Osler, J. C., & Algan, O. (1999). *A high resolution seismic sequence analysis of the Malta Plateau*.

Romagnoli, B., Grasselli, F., Costantini, F., Abbiati, M., Romagnoli, C., Innangi, S., Di Martino, G., & Tonielli, R. (2021). Evaluating the distribution of priority benthic habitats through a remotely operated vehicle to support conservation measures off Linosa Island (Sicily Channel, Mediterranean Sea). *Aquatic Conservation: Marine and Freshwater Ecosystems*, *31*(7), 1686–1699. https://doi.org/10.1002/aqc.3554

Rotolo, S. G., Castorina, F., Cellura, D., & Pompilio, M. (2006). Petrology and geochemistry of submarine volcanism in the Sicily Channel Rift. *The Journal of Geology*, *114*(3), 355–365. https://doi.org/10.1086/501223

Ruiz, C. R., García-Cacho, L., Araña, V., Luque, A. Y., & Felpeto, A. (2000). Submarine volcanism surrounding Tenerife, Canary Islands: Implications for tectonic controls, and oceanic shield forming processes. *Journal of Volcanology and Geothermal Research*, *103*(1-4), 105–119. https://doi.org/10.1016/S0377-0273(00)00218-3

Spatola, D., Micallef, A., Sulli, A., Basilone, L., & Basilone, G. (2017). Gathering different marine geology data (seismics, acoustics, sedimentological) to investigate active fluid seepage (AFS) in the Southern Region of the Central Mediterranean Sea. *IMEKO TC19 Workshop on Metrology for the Sea, MetroSea 2017: Learning to Measure Sea Health Parameters*.

Spatola, D., Micallef, A., Sulli, A., Basilone, L., & Basilone, G. (2018a). Evidence of active fluid seepage (AFS) in the southern region of the central Mediterranean Sea. *Measurement*, *128*, 247–253. https://doi.org/10.1016/j.measurement.2018.06.058

Spatola, D., Micallef, A., Sulli, A., Basilone, L., Ferreri, R., Basilone, G., Bonanno, A., Pulizzi, M., & Mangano, S. (2018b). The Graham Bank (Sicily Channel, central Mediterranean Sea): Seafloor signatures of volcanic and tectonic controls. *Geomorphology*, *318*, 375–389. https://doi.org/10.1016/j.geomorph.2018.07.006

Spatola, D., Sulli, A., Casalbore, D., & Chiocci, F. L. (2021). First evidence of Contourite drifts in the North-Western Sicilian active continental margin (Southern Tyrrhenian Sea). *Journal of Marine Science and Engineering*, *9*(10), 1043. https://doi.org/10.3390/jmse9101043

Sulli, A., Zizzo, E., Spatola, D., Morticelli, M. G., Agate, M., Iacono, C. L., Gargano, F., Pepe, F., & Ciaccio, G. (2020). Growth and geomorphic evolution of the Ustica volcanic complex at the Africa-Europe plate margin (Tyrrhenian Sea). *Geomorphology*, *374*, 107526. https://doi.org/10.1016/j.geomorph.2020.107526

Todaro, S., Sulli, A., Spatola, D., Basilone, G., & Aronica, S. (2022). Seismic stratigraphy of the north-westernmost area of the Malta Plateau (Sicily Channel): The Middle Pleistocene-Holocene sedimentation in a tidally

influenced shelf. *Marine Geology*, 106740. https://doi.org/10.1016/j.margeo.2022.106740

Todaro, S., Sulli, A., Spatola, D., Micallef, A., Di Stefano, P., & Basilone, G. (2021). Depositional mechanism of the upper Pliocene-Pleistocene shelf-slope system of the western Malta Plateau (Sicily Channel). *Sedimentary Geology*, *417*, 105882. https://doi.org/10.1016/j.sedgeo.2021.105882

Uchupi, E., Swift, S., & Ross, D. (1996). Gas venting and late Quaternary sedimentation in the Persian (Arabian) Gulf. *Marine Geology*, *129*(3-4), 237–269. https://doi.org/10.1016/0025-3227(96)83347-0

Washington, H. S. J. (1909). The Submarine Eruptions of 1831 and 1891 near Pantelleria. *American Journal of Science*, *27*(158), 131.